Organoclay/thermotropic liquid crystalline polymer nanocomposites. Part II: shear-induced phase separation

Youhong Tang · Ping Gao · Lin Ye ·
Chengbi Zhao · Wei Lin

Abstract Experimental studies on a kind of thermotropic liquid crystalline polymer (TLCP) containing 30% *p*-hydroxybenzoic acid (HBA), 35% hydroquinone (HQ), and 35% sebacic acid (SA) in mole fractions and its nanocomposite (TC3) containing 3.0 wt% organoclay are reported. The structures and dynamics of shear-induced phase separation and the effects of these structures on the macroscopic rheological properties of the nanocomposite are characterized under different shear conditions at 190 °C, which is in the nematic transition region of TLCP. The molecular level interactions between organoclay and TLCP molecules form a percolated-network structure in the composite, causing the composite to display complex viscosity with more than two orders of magnitude greater than that of TLCP in linear regions. However, such a network structure is easily destroyed in steady shear deformation, and it does not recover. Polarized optical microscopy (POM) equipped with a Cambridge shear system and transmission electron microscopy (TEM) confirm a shear-induced phase separation phenomenon during steady shear deformation. Two phases are observed in POM and TEM, with TLCP-rich and organoclay-rich phases. Steady shear at a small shear rate is effective to separate the two phases for characterizations.

Y. Tang (✉) · P. Gao
Department of Chemical and Biomolecular Engineering,
The Hong Kong University of Science and Technology,
Clear Water Bay, Kowloon, Hong Kong, China
e-mail: youhongtang@gmail.com

P. Gao
e-mail: kepgao@ust.hk

L. Ye
Centre for Advanced Materials Technology, School
of Aerospace, Mechanical and Mechatronic Engineering,
The University of Sydney, Sydney, NSW 2006, Australia

Y. Tang · C. Zhao · W. Lin
Centre for Advanced Marine Materials, School of Civil
Engineering and Transportation, South China University
of Technology, Guangzhou 510641, China

Introduction

It has long been known that shear can change the structure of multiphase polymer melt systems at different levels. The interplay of structure and rheology can be important in determining polymer melt properties and its processability. The properties of multiphase polymer melt systems are to a large extent affected by the morphology, which in turn depends on the thermodynamic, rheological, and interfacial properties of constituent components, the composition and the mixing conditions. To elaborate the strong structure–property relationship of these systems, considerable efforts have been devoted to comprehensive increased knowledge of how to control morphology of polymer melt systems during processing. The rheology of fluid dispersion has received considerable attention, and good reviews are available [1–3]. Structural studies of dispersion under flow are generally undertaken by optical [4] and scattering studies of shear-induced order [5] and by computer simulation [6]. Recent work includes, for example, some studies of polymeric [7] and surfactant fluids [8]. There is also fundamental interest in the problem of phase separation under shear [9].

Optical microscopy has already been used to study the flow behavior of a dispersion of plate-like particles. A sample of hexagonal disks of nickel hydroxide stabilized with a short-chain, charged polymer was investigated over a range of shear rates up to 100 s^{-1} with polarized transmitted light microscopy. These results were compared with studies using rheological measurement, scattering and diffraction [10]. This model system complements work on the flow with other plate-like particles such as clays [11–13] that are more polydispersed and often have complex inter-particle interactions.

The knowledge about the rheological and structural characteristics of liquid crystalline polymers (LCPs) has increased substantially during the last two decades. The properties of LCPs are strongly influenced by flow-induced molecular orientation during processing. In addition, adding fillers is a standard method of reducing the cost of expensive materials such as LCPs. Using fillers can be a useful route to reduce the sometimes very high level of anisotropy encountered in LCPs [14]. Understanding the effect of the presence of particles on the rheology of LCPs is not a trivial matter as the particles can interact with the liquid crystalline structure in various ways. Only very limited data on filled LCPs are available in the literature [15–18].

This study examines the structures and dynamics of flow-induced phase separation and the connection of these structures to the macroscopic rheological properties of a thermotropic liquid crystalline polymer (TLCP)/organoclay nanocomposite. To accomplish this, polarized optical microscopy (POM) and transmission electron microscopy (TEM) were performed to evaluate the flow-induced phase separation structures, and mechanical rheometer was used to characterize rheological properties of the nanocomposite.

Experiments

Materials

TLCP, a copolyester containing 30% *p*-hydroxybenzoic acid (HBA), 35% hydroquinone (HQ) and 35% sebacic acid (SA), has been described previously [19]. The clay, Closite 20A, modified by dimethyl dihydrogenated tallow ammonium ions, was kindly supplied by Southern Clay Products. The nanocomposite (TC3) with 3 wt% content of organoclay in TLCP was prepared by ultra-sonication, centrifugation, and solution casting methods, which has already been evaluated in previous studies [20].

Wide angle X-ray diffraction (WAXRD)

WAXRD was conducted at ambient temperature using a Philips powder X-ray diffraction system (Model PW 1830,

The Netherlands). WAXRD was conducted with Cu Kα radiation of wavelength 1.5406 Å.

Fourier transform infrared spectroscopy (FTIR)

A FTIR spectrometer (Bio-Rad FTS 6000, USA) was used at ambient temperature with a liquid cell container for the solutions. Spectral resolution was maintained at 2 cm^{-1}. Dry nitrogen gas was used to purge the sample compartment to reduce interference of water and carbon dioxide in the spectrum. The solutions were the TLCP/chloroform and the TLCP/organoclay/chloroform solutions before the evaporation procedure.

Transmission electron microscopy (TEM)

All samples were ultra-microtomed with glass knives on a Leica ultracut microtome (Leica ultracut-R ultramicrotome, Germany) at ambient temperature to provide sections with a nominal thickness of 100 nm and cut speed of 1.6 mm/s. TEM images were obtained with a transmission electron microscope at 200 kV (JEOL 2010, Japan).

Rheological measurement

Controlled strain rheological measurements were carried out using Advanced Rheometric Expansion System (ARES) (TA instruments, USA). 50 mm cone and plate fixtures with nominal cone angle 0.1 rad and nominal gap 0.0508 mm were used for all tests reported here. All measurements were performed at 190 °C with a 2000 g-cm transducer within the resolution limit of 0.2 g-cm and a 200 g-cm transducer within the resolution limit of 0.02 g-cm. Before testing, the samples were preheated and equilibrated at the test temperature for at least 30 min.

Polarized optical microscopy (POM)

The mesophase structures of the liquid-crystalline phase of TLCP and TC3 were investigated by POM using an Olympus microscope BX 50 with a Cambridge shear system CSS450 connecting a hot stage (Linkam Scientific Instruments, UK). The outstanding feature of this setup is that it allows investigation of texture changes at different temperatures and under varying shear rates. Mesophase structure images were obtained at 190 °C after preshearing samples at a low shear rate, i.e. 0.5 s^{-1}, for more than 3600 s to remove any shear history and anchored defects, and to provide a common shear history or structure to the samples before they were rested isothermally for a sufficient time. The images were also obtained at 230 °C after shear at 0.5 s^{-1} for 1800 s and relaxation to a steady state.

Results

Ultrasonication effects

The kinetics of solution casting with ultrasonication, observed by tracing the evolution over the time of WAXRD diffraction patterns for the solutions of TLCP with organoclay in chloroform are exhibited in Fig. 1. From the WAXRD patterns, it is clear that originally, the organoclay had d-spacing of 2.35 nm but after just 10.0 min sonication the peak position shifted dramatically to a lower angle with corresponding d-spacing of 3.92 nm, and broad shoulders rather than peaks appeared after 20.0 min, which may indicate that fully exfoliated morphologies were formed in solution form after sonication for 20.0 min, though in real experiment, the sonication process went up to 2.0 h.

IR spectroscopy is very sensitive to polymer microstructure and has been widely used in investigations of hydrogen bonding, macromolecular orientation, and crystallinity in polymer materials. Figure 2 gives the FTIR spectra of chloroform solutions with TLCP and TC3 before and after ultrasonication. It can be seen in Fig. 2 that the peak at the wavenumber of 1045 cm^{-1} for TLCP and TC3 before sonication shifted to the wavenumber of 1065 cm^{-1} after sonication (as marked with "*" in Fig. 2), and the intensity of the corresponding peaks, 1015, 1160, 1180, and 1260 cm^{-1}, increased after sonication was introduced into the fabrication procedure.

Here, 1015 and 1260 cm^{-1} represent the –C–O– group and 1160 and 1180 cm^{-1} represent the –C=O group in the TLCP molecules. After sonication, the relative intensities of those peaks increased, indicating that more ordered structures formed after sonication. The absorption peak at 1045 cm^{-1} is believed to represent the –C–O– group in the TLCP molecules, the peak shift be in the result of weak interaction between the positively charged N^{+} ion in the

Fig. 2 FTIR spectra of TLCP in chloroform and TLCP/organoclay (weight ratio = 97/3) in chloroform before and after sonication for 2.0 h

surfactant 2M2HT existing at the surface of the organoclay with the –C–O– group in TLCP molecules. The above observations are very important for interpreting the special properties of the hybrid.

Dispersion of organoclay

The structures and morphologies of polymer–organoclay nanocomposites depend on polymer interaction with organoclay and dispersion of organoclay in the polymer matrix. The position of the (001) plane diffraction peak observed in the WAXRD pattern can be used to determine the interlayer distance of organoclay layers according to the Bragg equation, i. e., $\lambda = 2d\sin\theta$, where λ is the wavelength of X-ray, d is the spacing between the planes measured, and θ is the angle between the incident ray and the scattering planes. The (001) plane diffraction peak observed from the WAXRD pattern of TC3 decreased in angle and exhibited a plateau rather than a sharp peak, compared with the diffraction peak of organoclay as shown in Fig. 3. This suggests that the spaces between the layers in TC3 have become larger than the space of organoclay and formed a partially intercalated structure in TLCP matrix.

The TEM images of TC3 presented in Fig. 4a, b provide direct observation of organoclay morphologies in TLCP matrix. Figure 4a is a global view of the TC3 nanocomposite. Organoclay is well dispersed in the TLCP matrix with some agglomeration of the size of ∼50 nm. Figure 4b shows high magnification images of TC3 nanocomposites, which indicate that organoclay formed partially intercalated structures with d-spacing averaging approximately 4–5 nm; the existence of the broad shoulder in the TC3 WAXRD pattern shown in Fig. 3 should be attributed to these nonexfoliated layers, which lie parallel within the agglomerated layers.
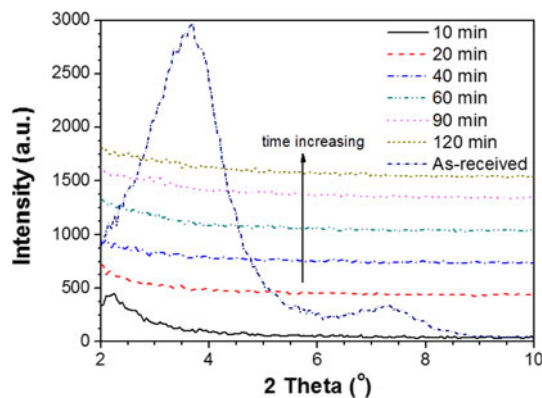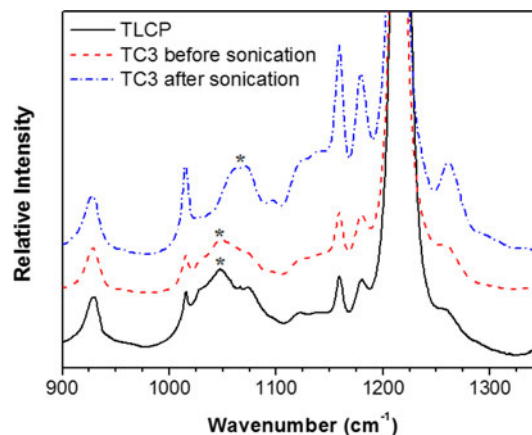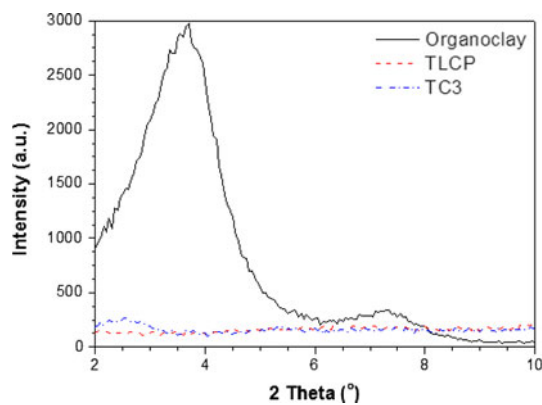

Fig. 1 Wide angle X-ray diffraction patterns of TLCP/organoclay (weight ratio = 97/3) in chloroform solution with different ultra sonication times

Fig. 3 Wide angle X-ray diffraction patterns of organoclay, TLCP, and TLCP/organoclay nanocomposite (TC3) at ambient temperature

From WAXRD and TEM, we conclude that this organoclay forms hybrid intercalated and exfoliated structures with good dispersion in the main-chain TLCP matrix.

Rheological behaviors

The TLCP used here has a number of advantages over other LCPs [19–22]. (1) It has a low transition temperature, being fully nematic at about 190 °C; (2) the fully nematic window is small, 180–192 °C; and (3) it displays a number of phenomena of interest, dependent on temperature and preparation, e.g., temperature dependent critical shear strains [20]. It has already been reported [21] as an excellent viscosity reducing agent for polyethylene, with reduction in viscosity of 89–94%.

The transition from linear to nonlinear viscoelastic behaviors, as manifested in dynamic strain sweep experiments, for TLCP and TC3, is shown in Fig. 5 with three different conditions: (i) the as-received sample (called "without preshear"); (ii) the as-received sample with steady shear at 0.5 s^{-1} for 3600 s (called "with preshear"); and (iii) the as-received sample with steady shear at 0.5 s^{-1}
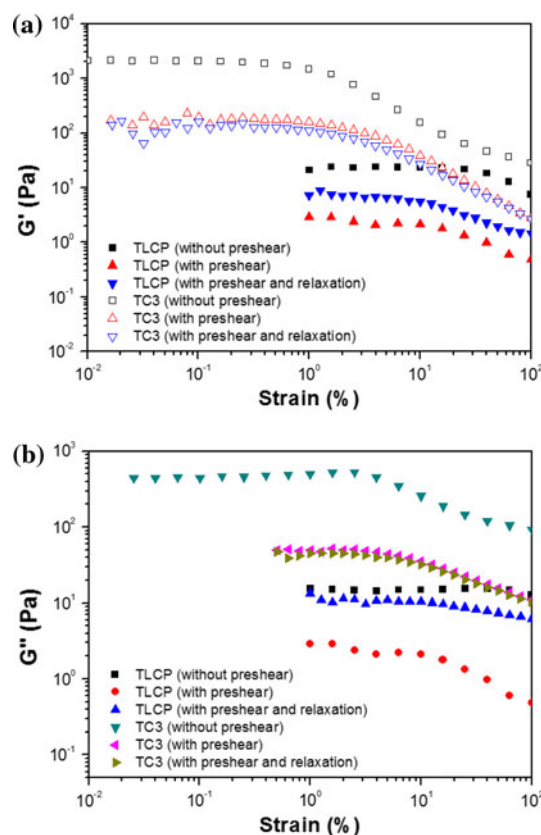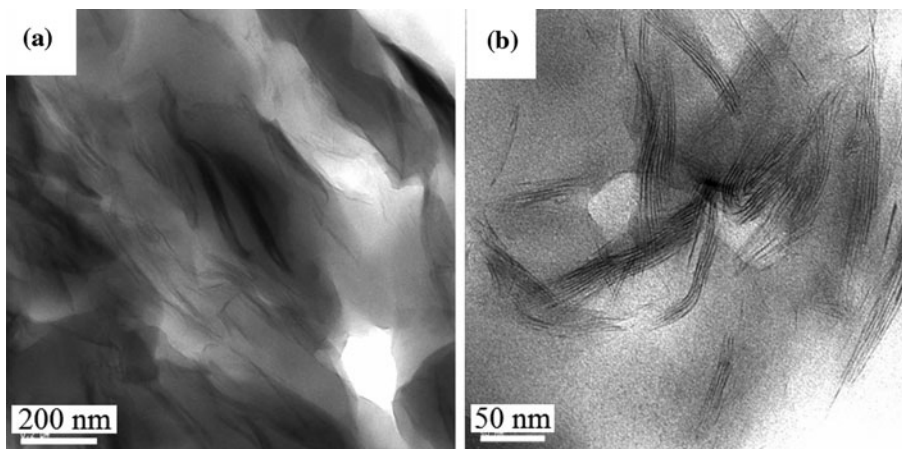

Fig. 5 a Storage and **b** loss modulus in dynamic strain sweep at 190 °C for TLCP and TLCP/organoclay nanocomposite (TC3)

for 3600 s followed by relaxation for 3600 s (called "with preshear and relaxation").

In Fig. 5a, b, for the without preshear sample, it can be seen that TC3 shows an increase of two orders of magnitude in dynamic storage modulus, G', and dynamic loss modulus, G'', in comparison with the matrix polymer in the linear viscoelastic region where the strain amplitude is below the critical value. On the other hand, G' and G'' exhibit the expected shear-thinning behavior, with the

Fig. 4 TEM images of TLCP/organoclay nanocomposite (TC3) before shear with different magnifications

critical strain amplitude for the transition decreasing dramatically from about 20.0 to 1.0% with only 3 wt% organoclay loading. Furthermore, the strain amplitude dependence of storage modulus in the shear-thinning regime increases with the addition of organoclay.

In the nematic phase, the textures of TLCP are very stable, giving a very large linear viscoelastic response region, as shown in Fig. 5. Because the organoclay layers disperse into the polymeric matrix as a few organoclay layers or stacks of layers which are randomly organized under the quiescent condition, it is expected that in the quiescent state, a greater proportion of the layers or stacks would be hydro-dynamically hindered, resulting in the filler–filler interaction becoming important and in fact dominating the long-term viscoelasticity of the composites. Additionally, with organoclay, the ease with which the organoclay structure can be altered by flow is considerably enhanced primarily because of filler–filler interactions. It is not surprising, then, that the threshold strain amplitude for the onset of shear-thinning decreases with additional organoclay and the strain amplitude dependence of the shear thinning is enhanced for the nanocomposite.

Comparing the same sample with different conditions, for the TLCP samples, in the linear region, $G'_{\text{without preshear}} > G'_{\text{with and relaxation}} > G'_{\text{with preshear}}$ which means that after relaxation for 3600 seconds, partial recovery of the TLCP molecules occurs. For the critical strain, $\gamma_{\text{without preshear}} > \gamma_{\text{with preshear}} > \gamma_{\text{with preshear and relaxation}}$. With preshear, the critical strain decreases and does not recover, but the TLCP molecules recover partially within 3600 seconds, which is due to the fact that the molecular network formed by the less-than-rigid molecular chains in the semiflexible LCPs was broken during the preshear procedure. For the TC3 samples, $G'_{\text{without preshear}} > G'_{\text{with preshear and relaxation}} \cong G'_{\text{with preshear}}$ and the critical strain $\gamma_{\text{without preshear}} < \gamma_{\text{with preshear}} \cong \gamma_{\text{with preshear and relaxation}}$. No recovery occurs within the 3600 s relaxation period for the TC3 storage modulus, and the critical strain increases slightly after preshear.

Dynamic frequency sweep was used to further characterize the rheological behaviors in the linear regions for TLCP and TC3. The dynamic modulus dependence on frequency shown by Fig. 6 was also measured in the above three conditions. As evident in Fig. 6a, for the TLCP sample without preshear, in the low frequency region G' is nearly independent of frequency, suggesting the possibility of pseudo-solid-like behavior for time scales at least of the order of 10^2 s. These local correlations cause the presence of domains and the presence of these domains causes the enhanced low-frequency modulus and the related low power-law dependence. For the TC3 nanocomposite without preshear, there is an increase more than two orders of magnitude in G' compared to that of TLCP. Across all measured frequencies, G' of TC3 is nearly independent of
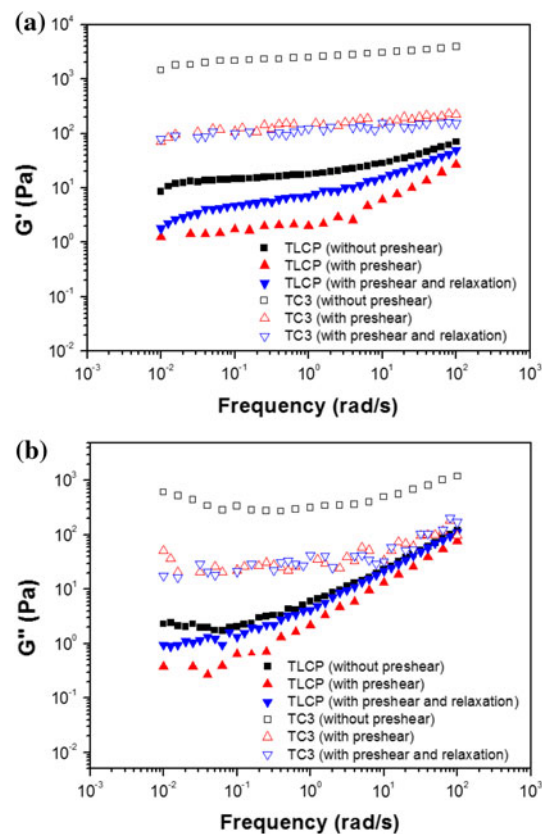

Fig. 6 a Storage modulus G' and **b** loss modulus G'' in dynamic frequency sweep at 190 °C for TLCP and TLCP/organoclay nanocomposite (TC3)

frequency, and an even more solid-like structure is produced than that of TLCP. The results of dynamic frequency sweep for preshear and for preshear and relaxation are also shown in Fig. 6. Both the storage and loss modules are considerably lower than those of the as-received sample. As seen in Fig. 6a, G' for the sample with preshear and relaxation shows the trend from that of the with preshear sample to that of the without preshear sample as frequency increases, indicating that the TLCP molecules try to recover their original condition during the time of the experiment; G'' recovers fully to its original state, as shown in Fig. 6b. The most dramatic discovery is that the sample with preshear and the sample with preshear and relaxation have the similar G' and G'' values for TC3, as presented in Fig. 6, which clearly shows that the with preshear and relaxation sample contains the same structures as the with preshear sample. The above analysis obviously leads to the conclusion that large strain can destroy the percolated network structures in the TC3 nanocomposite and the structures cannot recover their original form.

The frequency, ω, dependence of G' for the preshear sample is much stronger than the as-received sample for TLCP. As shown in Fig. 6a, the plot of $G'-\omega$ has a

different shape in the lower frequency region for TLCP, indicating that after preshear, the solid-like phenomenon which existed in the original sample can be weakened. For TC3 there is no marked difference between the three conditions. G' still shows the near frequency independence phenomenon. The curves just shift more than one magnitude lower and parallel with original TC3 curve. It seems that the solid-like phenomenon still exists in the preshear TC3 nanocomposite with the similar structures and relatively lower G' and G'' than the original sample.

With regard to dynamic oscillatory shear, it is clear that the addition of organoclay has a profound influence on the long-term relaxation behavior of TC3. With the addition of organoclay, TC3 shows a two order of magnitude increase in G' compared to TLCP, and the reason for these observed phenomena is the temporal network structures. After large strains are imposed, the structures formed in TC3 cannot recover their original form.

Discussion

POM images with low magnification indicated that clear agglomerations existed after shear at 190 °C, as shown in Fig. 7a. Shear-induced phase separation occurred producing two phases: a TLCP-rich phase and an organoclay-rich phase. Figure 7b, c shows POM images of TC3 at high magnification. Semi-solid materials can be detected in the organoclay-rich phase. The TLCP-rich phase shows a monodomain with a few defect structures, similar to the texture of pure TLCP in the nematic state. Figure 7d–f shows the POM images of TC3 after steady shear with a shear rate 0.5 s^{-1} for 1800 s at 230 °C, where pure TLCP gives isotropic–nematic biphase structures. Figure 7d presents a clear image of isotropic–nematic biphase structures in the TLCP-rich phase and a semi-solid structure in the organoclay-rich phase. Figure 7e, f shows detailed images of the two phases. TEM images of TC3 after shear are shown in Fig. 8. Direct comparison with the TEM images of the as-received TC3 sample (Fig. 4) shows clearly that after shear, a two-phase structure exists with the organoclay agglomerated and forming lumps of a size ∼100 nm.
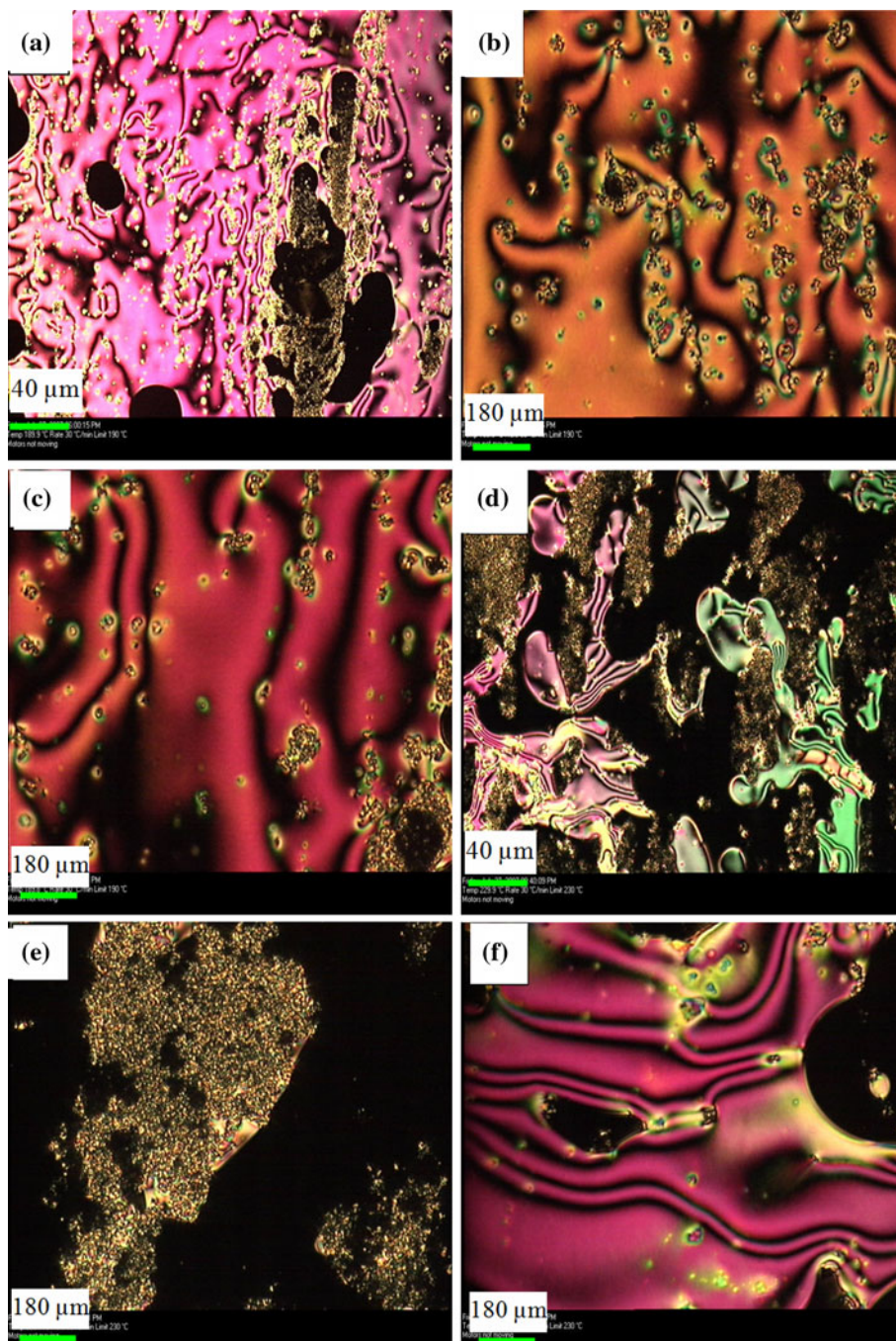
Several theories have been proposed to describe the interactions and coalescence of particles. A comprehensive treatment of the subject is given in a review by Chesters [23]. The theories of coalescence are based on either equilibrium thermodynamics or hydrodynamics; the former considers quiescent systems in which coalescence results from minimization of the total free energy by reduction of the interfacial area, whereas the latter addresses flowing systems. Although the major mechanisms of collision and coalescence of particles are considered to be flow, the effect may also take place in quiescent systems. The proposed mechanisms in the quiescent condition originate from Brownian motion, dynamics of concentration fluctuation, sedimentation, temperature gradients, etc. Some of these effects may also present during flow and they may be either enhanced or suppressed by flow. However, considering the relatively high viscosity and large particles present in polymer blends, Brownian motion can scarcely play a major role in coalescence since particle diffusion is inversely related to particle diameter and matrix viscosity. A mechanism likely to occur in polymer blends is the so-called Ostwald ripening [24, 25]: large particles grow at the expense of small ones by diffusion of molecules from the small particles with high interfacial energy to the larger ones. This process is enhanced by flow and can be described by a scaling law. It is experimentally established and commonly recognized that the dispersed particles in dispersive multiphase polymer systems, their size, and distribution are the result of a competitive process between break-up and coalescence. Under given flow conditions, an invariant morphology can be attained that represents a balance between particle break-up and flow-induced coalescence. The larger particles are deformed and broken up by the stresses of the flow field, while concurrently particles collide and fuse to temporarily form larger domains.

From the above examination, using phase separation phenomenon in the complex, TC3 nanocomposite by continuous shearing can effective separated TC3 into two simple systems (TLCP-rich and organoclay-rich phases). Step rate tests were performed to elucidate the phase separation condition with high efficiency.

Figure 9a shows the transient shear stress evolution for TLCP and TC3 in preshear condition (steady shear at a shear rate 0.5 s^{-1} for 3600 s and relaxation for 3600 s). Figure 9a shows that both TLCP and TC3 had one broad overshoot before reaching a steady state. For TLCP, it is suggested that the overshoot was due to chain stretching and shear-induced demixing, as reported by Magda et al. [26] for dioctyl phthalate of high molecular weight polystyrene. There was a large difference between the overshooting values of the two materials, with the TC3 displaying an overshooting value almost 20 times higher than TLCP. However, a much smaller difference existed between the steady state values, with TC3 displaying only approximately the twice stress value of TLCP. The normalized stresses for TLCP and TC3 are shown in Fig. 9b. For TLCP, the maximum overshooting value was approximately three times as high as the steady state value, while the TC3 nanocomposite it was more than 25 times higher. One reason for the substantial difference between the overshoot and steady state values for the nanocomposite was the permanent destruction of the temporary network structures that originally existed in the nanocomposite. Another reason was the phase separation during continuous

Fig. 7 POM images of TLCP/
organoclay nanocomposite
(TC3). **a–c** After shear 0.5 s^{-1}
for 3600 s and relaxation at
190 °C and **d–f** after shear
0.5 s^{-1} for 1800 s and relaxed
at 230 °C

shearing. Figure 10 shows the separated organoclay-rich phase and TLCP-rich phase after steady shear on the parallel plate fixture at 190 °C. The organoclay-rich phase had a semi-solid morphology and stuck to the testing fixtures during shear. It was lubricated by the TLCP-rich phase on its surface. Only the viscosity of TLCP-rich phase was measured, which represented the total measured viscosity.

The normalized shear stress evolution for TC3 with different shear rates at 190 °C is exhibited in Fig. 11 with large stress overshootings observed at different shear rates.

Ideally, if complete separation occurred, the steady shear viscosity of the nanocomposite is only contributed from TLCP-rich phase. In reality, more efficient phase separation would cause lower shear viscosity at steady state, which approaches to the viscosity of TLCP-rich phase under the same condition. Since the viscosity of TLCP-rich phase has not obtained at this stage, the ratio of the normalized shear stress values between the overshooting and steady state for the nanocomposite can be used to determine the efficiency of the separation. Larger ratio means higher different
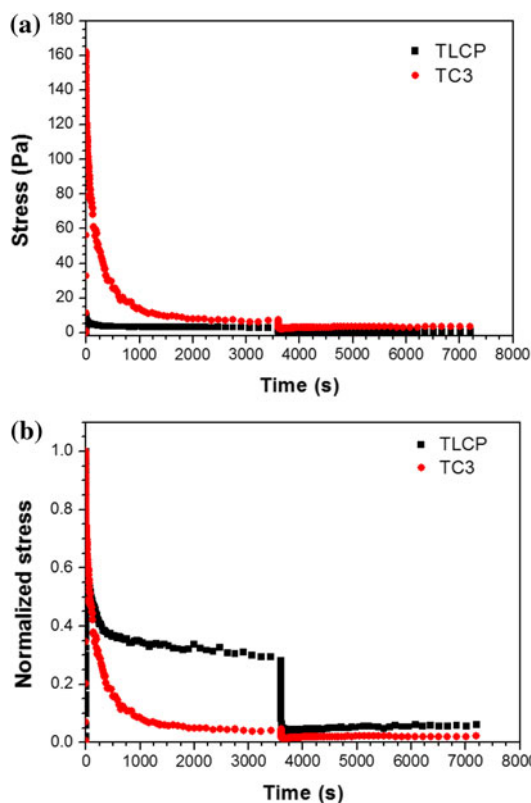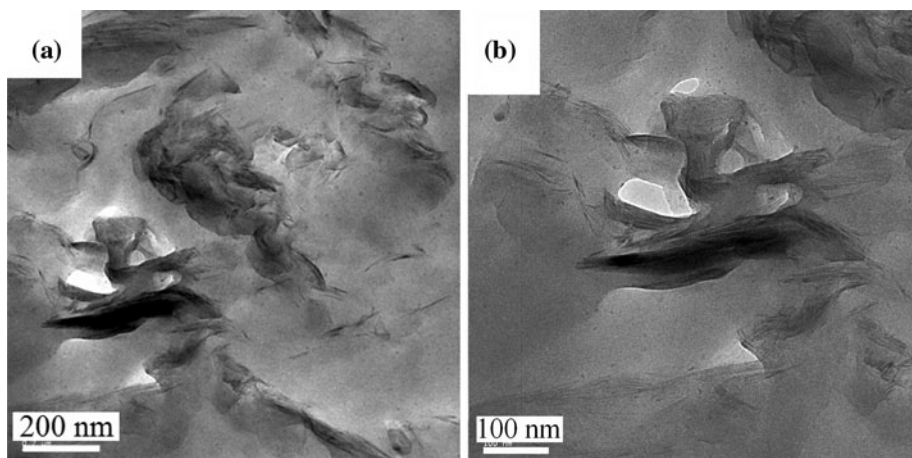
Fig. 9 **a** Stress and **b** normalized stress evolution during preshear condition with shear rate 0.5 s^{-1} for 3600 s and relaxation for 3600 s at 190 °C for TLCP and TLCP/organoclay nanocomposite (TC3)
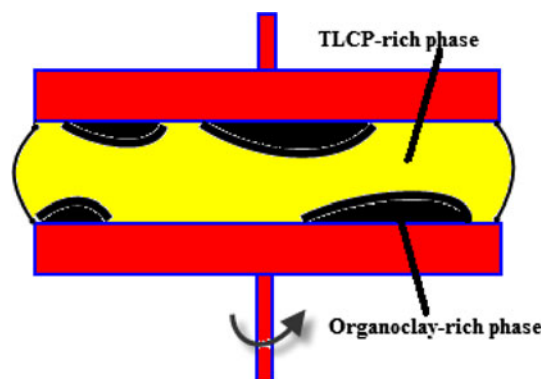

Fig. 10 Schematic drawing of separated TLCP-rich phase and organoclay-rich phase in TC3 after steady shear on mechanical rheometer the parallel plate fixture at 190 °C
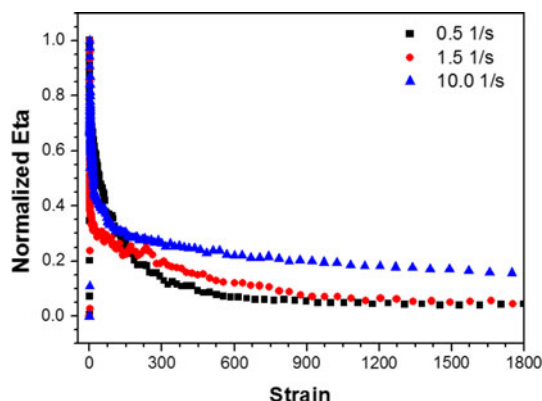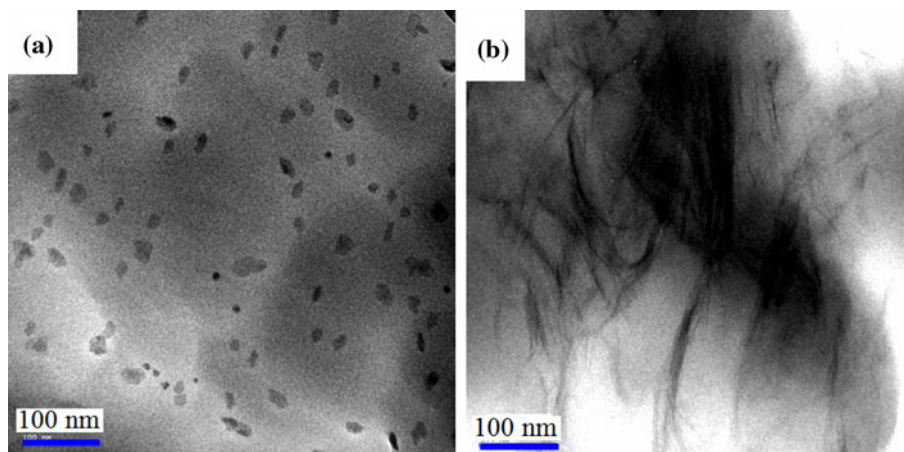

Fig. 11 Normalized stress evolution of TLCP/organoclay nanocomposite (TC3) under different shear rates at 190 °C

viscosity values between overshooting and steady state and more completely the percolation network structures been destroyed, so, more efficiently the phase separation occurred. Under the same shear strain, in the low shear rate condition (i.e. 0.5 s^{-1} and 1.5 s^{-1}), a much larger ratio obtained than at the high shear rate (i.e. 10.0 s^{-1}); e.g., at 0.5 s^{-1}, the ratio was about 25, whereas at 10.0 s^{-1} the ratio was only 11. Steady shear with low shear rates, e.g., 0.5, 1.5 s^{-1} could efficiently separate the two phases.

Figure 12 shows TEM images of TC3 separated by capillary rheometer at 190 °C with a low shear rate (5.0 s^{-1}). It separated into TLCP-rich material, as shown in Fig. 12a (organoclay uniformly dispersed in TLCP matrix with size 15–25 nm and formed exfoliated structures) and organoclay-rich material, as shown in Fig. 12b (organoclay

Fig. 12 TEM images of
a polymer-rich and
b organoclay-rich phases after
separation process for TLCP/
organoclay nanocomposite
(TC3) at 190 °C with capillary
rheometer

formed intercalated structures in TLCP matrix with high concentrations). Repeated separation can be performed to obtain purer materials. After separation, the nanocomposite became much simpler to analyze. Different interactions of organoclays with the liquid crystalline structures are expected in these two different materials, which will cause different rheology behaviors in the systems. The detailed characterizations on these two materials will be further analyzed later.

Conclusions

When a small amount of organoclay was added into a TLCP matrix with a combination of ultrasonication, separation, and solution casting methods, organoclay formed partially intercalated structures, and molecular level interactions occurred between the two materials. Rheological characterization at 190 °C showed that a percolation network structure formed in the nanocomposite. With steady shear deformation of the nanocomposite, the percolated structure was destroyed and it did not recover. POM and TEM showed that a shear-induced phase separation phenomenon existed in the nanocomposite. A low shear rate (e.g. 0.5 s^{-1}) led to a more efficient phase separation phenomenon. By utilizing the shear-induced phase separation phenomenon, the nanocomposite can be separated into two materials (organoclay-rich phase and TLCP-rich phase) by steady shearing, and simpler structures can be obtained for further understanding the effects of organoclay on the rheology of TLCPs as the organoclay has different levels of interaction with the liquid crystalline structures.

References

1. Barnes HA, Hutton JF, Walters K (1989) Introduction to rheology. Elsevier, Amsterdam
2. Russel WB, Saville DA, Schowalter WR (1989) Colloidal dispersions. Cambridge University Press, Cambridge
3. Adams MJ, Mashelkar RA, Pearson AJ, Rennie AR (eds) (1998) Dynamic of complex fluids. Royal Society/Imperial College Press, London
4. Fuller GG (1995) Optical rheometry of complex fluid. Oxford University Press, New York
5. Rennie AR, Clarke SM (1996) Curr Opin Colloid Interface Sci 1:34
6. Ball RC, Merrose JR (1995) Adv Colloid Interface Sci 59:19
7. Krishnamoorti R, Silva AS, Modi MA, Hammouda B (2000) Macromolecules 33:3803
8. Escalante JI, Hoffmann H (2000) J Phys Condens Matter 12:A483
9. Lu CYD, Olmsted PD, Ball RC (2000) Phys Rev Lett 84:642
10. Brown ABD, Rennie AR (2001) Chem Eng Sci 56:2999
11. Ramsay JDF, Lindner P (1993) J Chem Soc Faraday Trans 89:4207
12. Pignon F, Magnin A, Piau JM (1997) Phys Rev Lett 79:4689
13. Brown ABD, Clarke SM, Convert P, Rennie AR (2000) J Rheol 44:221
14. Hongladarom K, Burghardt W (1993) Macromolecules 26:785
15. Zhang GL, Jiang CL, Su CY, Zhang HZ (2003) J Appl Polym Sci 89:3155
16. Chang JH, Ju CH, Kim SH (2006) J Polym Sci B 44:387
17. Huang WY, Han CD (2006) Macromolecules 39:257
18. Huang WY, Han CD (2006) Polymer 47:4400
19. Gao P, Lu XH, Chai CK (1996) Polym Eng Sci 36:2771
20. Tang YH, Gao P, Ye L, Chao CB, e-Polymer (submitted for publication)
21. Chan CK, Whitehouse C, Gao P (1999) Polym Eng Sci 39:1353
22. Chan CK, Gao P (2005) Polymer 46:10890
23. Chesters AK (1991) Chem Eng Res Des 69:259
24. Baldan A (2002) J Mater Sci 37:2171. doi:10.1023/A:1015388912729
25. Kabalnov A (2001) J Disper Sci Technol 22:1
26. Magda JJ, Lee CS, Muller SJ, Larson RG (1993) Macromolecules 26:1696